DETAILED ABUNDANCE ANALYSIS OF A METAL-POOR GIANT IN THE GALACTIC CENTER

N. Ryde[1], T. K. Fritz[2], R. M. Rich[3], B. Thorsbro[1], M. Schultheis[4], L. Origlia[5], and S. Chatzopoulos[6]
[1] Lund Observatory, Department of Astronomy and Theoretical Physics, Lund University, Box 43, SE-221 00 Lund, Sweden; ryde@astro.lu.se
[2] Department of Astronomy, University of Virginia, 3530 McCormick Road, Charlottesville, VA 22904, USA
[3] Department of Physics and Astronomy, UCLA, 430 Portola Plaza, Box 951547, Los Angeles, CA 90095-1547, USA
[4] Observatoire de la Côte d'Azur, CNRS UMR 7293, BP4229, Laboratoire Lagrange, F-06304 Nice Cedex 4, France
[5] INAF—Osservatorio Astronomico di Bologna, Via Ranzani 1, I-40127 Bologna, Italy
[6] Research Center for Astronomy, Academy of Athens, Soranou Efessiou 4, GR-115 27 Athens, Greece
Received 2016 June 21; revised 2016 August 18; accepted 2016 August 19; published 2016 October 26

ABSTRACT

We report the first results from our program to examine the metallicity distribution of the Milky Way nuclear star cluster connected to Sgr A*, with the goal of inferring the star formation and enrichment history of this system, as well as its connection and relationship with the central 100 pc of the bulge/bar system. We present the first high-resolution ($R \sim 24,000$), detailed abundance analysis of a $K = 10.2$ metal-poor, alpha-enhanced red giant projected at 1.5 pc from the Galactic center, using NIRSPEC on Keck II. A careful analysis of the dynamics and color of the star locates it at about 26^{+54}_{-16} pc line-of-sight distance in front of the nuclear cluster. It probably belongs to one of the nuclear components (cluster or disk), not to the bar/bulge or classical disk. A detailed spectroscopic synthesis, using a new line list in the K band, finds [Fe/H] ~ -1.0 and [α/Fe] $\sim +0.4$, consistent with stars of similar metallicity in the bulge. As known giants with comparable [Fe/H] and alpha enhancement are old, we conclude that this star is most likely to be a representative of the $\sim$10 Gyr old population. This is also the most metal-poor-confirmed red giant yet discovered in the vicinity of the nuclear cluster of the Galactic center. We consider recent reports in the literature of a surprisingly large number of metal-poor giants in the Galactic center, but the reported gravity of log $g \sim 4$ for these stars calls into question their reported metallicities.

Key words: Galaxy: center – stars: abundances – stars: late-type

1. INTRODUCTION

The predominance of late-type M giants in the bulge has been known since the work of Nassau & Blanco (1958) and in fact had marked the bulge as a metal-rich, disk population in the 1957 Vatican meeting on stellar populations. The evolved stellar content was known early on to be very different from that of the halo and globular clusters, even though Baade's (1951) discovery of RR Lyrae variables in the bulge offered one population in common. The lack of metal-poor giants with [Fe/H] ~ -1 was evident from the earliest abundance distributions (Rich 1988) and was confirmed in all subsequent studies (e.g., Fulbright et al. 2006; Zoccali et al. 2008; Johnson et al. 2011, 2013, 2014; Ness et al. 2013). While aspects of the microlensed dwarf population remain in debate, especially the age distribution, Bensby et al. (2013) agree with results based on giants in finding very few stars with [Fe/H] < -1. These studies all consider bulge fields with $b < -4°$, although the lack of a metal-poor population inward of $b = -4°$ continues to be confirmed in the GIBS survey (Gonzalez et al. 2015). Extremely metal-poor stars (e.g., [Fe/H] < -3) are known in the bulge, but they are so rare that wide-field surveys must be undertaken to discover them (see, e.g., Howes et al. 2015), and while they are in the bulge, they are considered to have an origin apart from most of the bulge (Koch et al. 2016). Simply based on an assessment of the nature of the bulge, known abundance gradients in external galaxies, and the well-established presence of massive clusters and young stars toward the Galactic center, it would be expected that few if any metal-poor stars might be found within 300 pc of the nucleus.

Indeed, at the Galactic center, Ramírez et al. (2000b), Carr et al. (2000), and Davies et al. (2009) found, by analyzing red supergiants, a metal-rich population narrowly distributed around the solar metallicity. Similar results are found by Ryde & Schultheis (2015) for M giants. Recently, though, Schultheis et al. (2015) found the presence of a metal-poor population beyond 70 pc from the nuclear cluster, which has a radius of approximately 7 pc (Fritz et al. 2016). Do et al. (2015) also reported a significant population of metal-poor stars in the nuclear cluster.

Here we report on the first high-resolution spectroscopy of a red giant with [Fe/H] ~ -1 to be found in the vicinity of the nuclear cluster, at a projected distance of 1.5 pc from the Galactic center. We have performed a detailed abundance analysis based on high-resolution, K-band spectra. Observing at K band makes such investigations possible due to the much lower extinction at higher wavelengths (Cardelli et al. 1989). The K-band extinction toward the central parsec is only $A_{K_S} = 2.74$ with a variation of ±0.30 due to spatial variations (Schödel et al. 2010).

2. TARGET SELECTION

We selected a list of Galactic center giants from spectra observed with the integral field spectrometer SINFONI (Bonnet et al. 2003; Eisenhauer et al. 2003) on the Very Large Telescope, providing a K-band resolution of $R = 4000$ or $R = 1500$. The selection for the target group, to which the observed star belongs, was done according to the following criteria: a K_S magnitude range of $10 < K_S < 11$, an angular distance from the Galactic center of R_c (Sgr A*) $> 25''$, and excluding stars with neighbors too close for seeing-limited high-resolution spectroscopy. Initially, SINFONI spectra were only used to ensure qualitatively that the objects are cool in the sense that the CO bandheads exist, but we have not imposed any initial cuts based on the CO band strength or derived
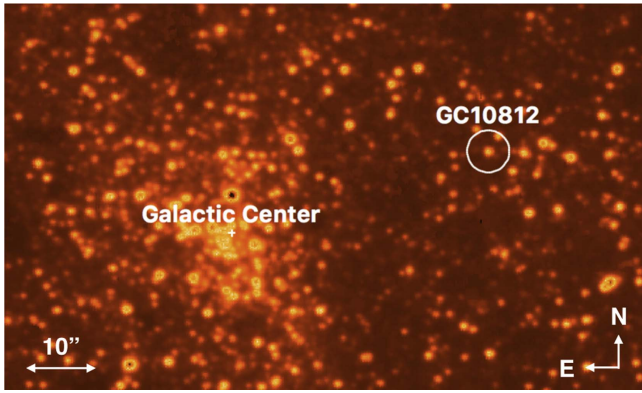
Figure 1. UKIDSS finding chart of the Galactic center (Lawrence et al. 2013). GC10812 is marked with a circle.

effective temperature. We also used the catalogs of Blum et al. (2003) and Matsunaga et al. (2009) to exclude some known asymptotic giant branch/long-period variable stars, such as Miras, and known red supergiants. The aim of this sample is to develop a relatively unbiased, large sample of old Galactic center stars that we will use in our study of the metallicity distribution. A more detailed discussion of our full sample is in preparation.

In Figure 1 we present a finding chart (Lawrence et al. 2013) with our observed target, the giant GC10812, indicated (see also Table 1). The star lies at an angular distance of $38{\farcs}4$ from the Galactic center. This corresponds to a projected galacto-centric distance of $R_c = 1.5$ pc, adopting the distance to the Galactic center of 8.3 kpc (Chatzopoulos et al. 2015a; Bland-Hawthorn & Gerhard 2016).

The K_S magnitude of GC10812 is 10.25 ± 0.05 from Nishiyama et al. (2009), and its color is $H - K_S = 1.63 \pm 0.07$. Using the extinction law of Fritz et al. (2011), this leads to an extinction of $A_{Ks} = 1.94 \pm 0.10$. The absolute magnitude of GC10812 is $M_{Ks} = -6.48 \pm 0.12$. This is close to the approximate tip of the RGB with $M_{bol} = -3.5$ (see also Tiede et al. 1995; Omont et al. 1999). Compared to all stars brighter than $M_{Ks} = -5.5$ from Nishiyama et al. (2009) within $100''$ of Sgr A*, the star is clearly bluer, -0.84 bluer than the median color. That means that only 21 of 1067 stars are bluer than GC10812. There are also extinction variations over the Galactic center (Schödel et al. 2010). To account for them, we measure relative color locally using Gemini AO data.[7] We use stars with $K_S < 16$ and account for intrinsic color differences. Dependent on the comparison scale ($3''$ or $6''$) and including other error sources like scatter and photometry uncertainty for the target, we obtain that GC10812 is 0.75 ± 0.10 bluer than the local median. Over the full Galactic center $3.6^{+2.7}_{-1.9}\%$ of all stars are that blue or bluer. The $H - K_S$ color excess corresponds to an extinction difference of $A_{Ks} = 1.01 \pm 0.14$ between the $A_{Ks} = 1.94$ measured for this star and $A_{Ks} = 2.95$ measured as the average for all stars in this region. That is more dust than the $A_{Ks} \approx 0.4$ that Chatzopoulos et al. (2015b) find within $r = 100''$ of Sgr A*. However, there is also extinction variation in the plane of sky (Schödel et al. 2010); at some places up to $A_{Ks} \approx 0.8$ was found. Further, the model of Chatzopoulos et al. (2015b) is very insensitive to dust at greater distances.

To constrain the line-of-sight position, we use the Galactic center model of Chatzopoulos et al. (2015a) and derive how much a star needs to be placed in front of Sgr A* in order for it to be bluer than $3.6^{+2.7}_{-1.9}\%$ of its stars. We obtain a distance of $D_c = 26^{+54}_{-16}$ pc. That is in principle a slight underestimate of the distance because the model includes no bar/bulge or Galactic disk. This contribution is, however, probably small; Launhardt et al. (2002) show that in this part of the nuclear disk the space density due to the bar/bulge is more than 40 times smaller than the contribution due to the nuclear disk. Its absolute extinction also argues for a location within the nuclear disk; an extinction of $A_{Ks} \approx 2$ is unusual for old stars outside the nuclear disk (Schultheis et al. 2014). Whether it is possible that the star still is around the outer rim of the nuclear cluster or not depends on the precise distance and nuclear cluster definition (Schödel et al. 2014; Chatzopoulos et al. 2015a; Fritz et al. 2016). It is, however, clear that the star is currently within a nuclear component, because the nuclear disk extends to an outer radius of 230 pc (Launhardt et al. 2002).

The dynamics measured in Fritz et al. (2016) are $\mu_l = 2.31 \pm 0.27$ mas yr^{-1}, $\mu_b = -3.12 \pm 0.27$ mas yr^{-1}, and $v_{rad} = -51 \pm 5$ km s^{-1} (which we confirm in our measurement of the star's heliocentric velocity from the NIRSPEC high-resolution spectra of -56.4 ± 1.0 km s^{-1}; see Table 1). These velocities are rather typical for a Galactic center star; see Figure 2. The positive velocity in l and the lower extinction fit as the extinction to a star in front of the Galactic center (Chatzopoulos et al. 2015b).

We calculate the orbit for the stars using the potential of Chatzopoulos et al. (2015a). This potential includes the supermassive black hole, nuclear cluster, and cluster disk. Three orbits are shown in Figure 3. For small current distances (black and red orbits in the figure) the average distance of GC10812 from the Galactic center is somewhat larger than the current distance from the Galactic center. That makes member-ship in the nuclear cluster unlikely, and excludes it nearly certainly if the cluster is assumed to have a Sérsic-like cutoff, which results in a half-light radius of about 5 pc (Schödel et al. 2014; Fritz et al. 2016). If it is instead assumed that the outer slope follows a power law (Chatzopoulos et al. 2015a), a membership in the nuclear cluster is still possible. When the star is currently at large distance (blue orbit in Figure 3), the star does not move much further away on its orbit. We conclude that the star most likely resides within the the nuclear disk and is unlikely to experience any excursions into the bulge or halo. We conclude based on the distance and kinematics that GC10812 is probably a nuclear disk star.

3. OBSERVATIONS

We observed the giant GC10812 on 2015 April 27 with the NIRSPEC spectrometer McLean (2005) mounted on Keck II, at a resolution of $R \sim 24,000$ in the K band, using the $0{\farcs}432 \times 12''$ slit and the NIRSPEC-7 filter. The retrieved spectra range from 21100 to 23300 Å, using five orders and therefore obtaining about 50% spectral coverage. We observed in an ABBA scheme with a nodding throw of $6''$ on the slit, to achieve proper background and dark subtraction. A total exposure time on target was 960 s. The data were reduced with the NIRSPEC software `redspec` (Kim et al. 2015), providing final 1D wavelength-calibrated spectra. IRAF (Tody 1993) was subsequently used to normalize the continuum, eliminate obvious cosmic-ray hits, and correct for telluric lines (with

---

[7] We use H-continuum and K (long) continuum images from program Gs-2013A-Q-15, avoiding data in which the target is saturated.

Table 1
Stellar Coordinates, Position, and Kinematics

Data	R.A. (h:m:s)	Decl. (d:m:s)	(l, b) (deg)	R_c (pc)	D_c (pc)	$v_{\rm rad}^{\rm helio}$ (km s^{-1})	μ_l (mas yr^{-1})	μ_b (mas yr^{-1})
GC10812	17:45:37.229	−29:00:16.62	(359.9, −0.035)	1.5	26	−56.5	2.31	−3.12
Uncertainties	⋯	⋯	⋯	±0.1	$^{+54}_{-16}$	±1.0	±0.27	±0.27
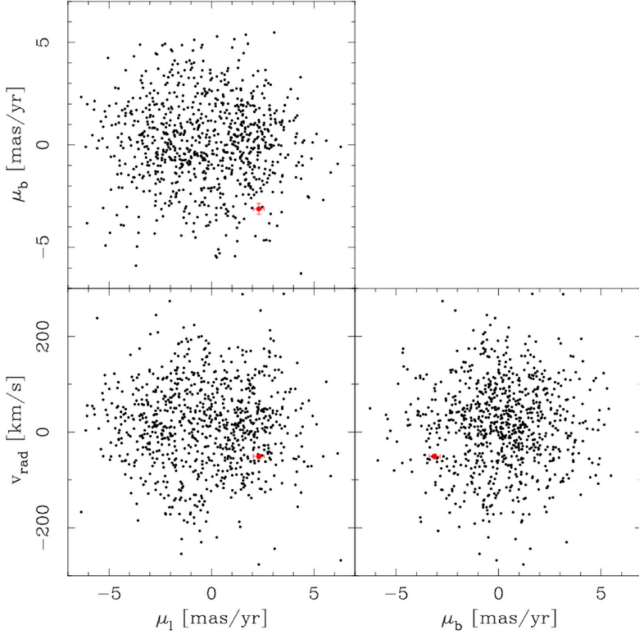
Figure 2. Velocity of GC10812 (red) in comparison with other Galactic center stars. The other stars are in 0.8–3.6 pc projected distance from Sgr A*.
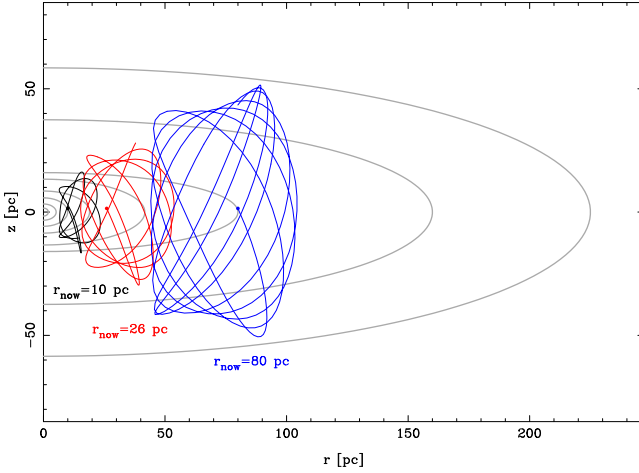

Figure 3. Orbit of GC10812. The red curve shows it for the most likely distance in front of the Galactic center (26 pc), while the other two curves show the orbit when the star would be at the outer/inner edge of the 1σ interval. The gray curves show equal star surface density of contours of the nuclear disk from Fritz et al. (2016) and Launhardt et al. (2002). The outermost curve marks roughly the outer edge of the nuclear disk.

telluric standard stars). We estimate S/N = 90 per pixel in our reduced spectra. A portion of the observed spectrum is shown in Figure 4.
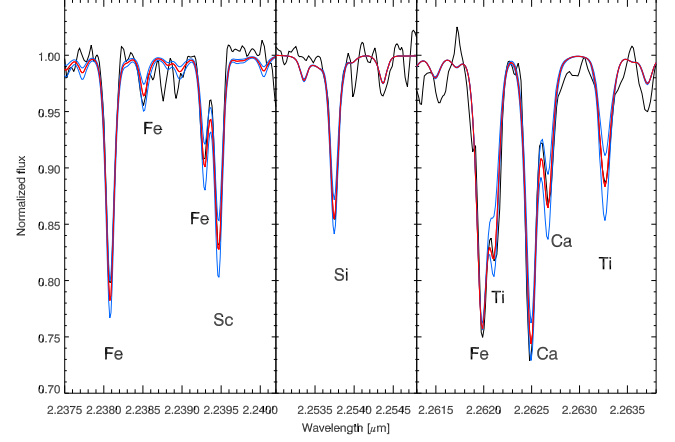

Figure 4. Examples of spectra covering a few of the lines used for the abundance determination. The black curves are the observations; the red one is the best-fit model. The blue spectra correspond to ±0.2 dex in the corresponding abundances, in order to show the sensitivity of these lines to the determined abundances.

4. ANALYSIS

We analyze our spectra, deriving detailed chemical abundances, by calculating synthetic spectra, given the star's fundamental parameters, i.e., effective temperature ($T_{\rm eff}$), surface gravity ($\log g$), metallicity ([Fe/H]), and microturbulence ($\xi_{\rm mic}$), and a suitable line list in the K band (see Section 4.2).

4.1. The Stellar Parameters

The derived $T_{\rm eff} = 3817 \pm 150$ K is determined from integrating the strength of the 2.3 μm CO (2–0) band in the SINFONI spectra[8] and using the relation between the CO band strength and the $T_{\rm eff}$ given in Schultheis et al. (2016). They have shown that this relation works very well in the temperature range between 3200 and 4500 K and in the metallicity range between 0.5 and −1.2 dex with a typical dispersion of about 150 K.

The surface gravity, $\log g$, is determined photometrically and assuming a mean distance of 8.3 kpc to the Galactic center, in the same manner as in Ryde & Schultheis (2015). A stellar mass of an old star of typically 1 $M_\odot$ is assumed, but the surface gravity is not very sensitive to the mass. A difference in mass of 0.2 $M_\odot$ gives 0.1 dex $\log g$ difference. In the calculation of the surface gravity we used the extinction law from Fritz et al. (2011) and the bolometric corrections from Houdashelt et al. (2000). An extinction uncertainty of $A_{Ks} = 0.1$ gives 0.2 dex error in $\log g$, and a bolometric uncertainty of $M_{\rm bol} = 0.12$ gives 0.15 dex uncertainty in $\log g$. The combined uncertainty is thus $\sqrt{0.1^2 + 0.2^2 + 0.15^2} = 0.27$ dex. Our derived surface gravity is thus $\log g = 0.5 \pm 0.3$ (dex).

---

[8] The SINFONI spectrum is from program 087.B-0117.

Table 2
Stellar Photometry, Parameters, and Abundances

Data	K_S	$H - K_S$	T_{eff} (K)	log g (dex)	ξ_{mic} (km s^{-1})	[Fe/H]	[Mg/Fe]	[Si/Fe]	[Ca/Fe]	[Ti/Fe]	[Sc/Fe]
GC10812	10.25	1.63	3817	0.5	2.0	−1.05	0.36	0.39	0.55	0.53	0.44
Uncertainties	±0.05	±0.07	±150	±0.3	±0.5	±0.1	±0.1	±0.1	±0.2	±0.3	±0.3

Ramírez et al. (2000a) found that the combination of the CO first-overtone band with the Na I and the Ca I lines is sensitive to the surface gravity of the star. We have therefore also measured the Na I and Ca I lines in the SINFONI spectra as in Schultheis et al. (2016). Our derived value for log[EW(CO)/(EW(Na) + EW(Ca))] = 0.405 for GC10812 locates our star on the RGB sequence of Ramirez et al. (1997).

We have chosen a typical value of $\chi_{mic} = 2.0 \pm 0.5$ km s^{-1} found in detailed investigations of red giant spectra in the near-IR by Tsuji (2008); see also the discussion in Cunha et al. (2007).

The location of GC10812 in the Hertzsprung–Russel diagram, using our derived effective temperature, surface gravity, and metallicity (see Table 2), is plotted with a big star symbol in Figure 5. It fits nicely on the red giant branch.

4.2. Line List

An atomic line list based on the VALD3 database (Piskunov et al. 1995; Kupka et al. 1999, 2000; Ryabchikova et al. 1997, 2015) has been constructed (B. Thorsbro et al. 2017, in preparation). Wavelengths and line strengths (astrophysical log gf-values) are updated for 575 lines in the K band using the solar center intensity atlas (Livingston & Wallace 1991). New laboratory measurements of wavelengths and oscillator strengths of Sc lines (Pehlivan et al. 2015) and newly calculated oscillator strengths of Mg lines (A. Pehlivan et al. 2016, in preparation) are included. ABO[9] line-broadening theory is included (Anstee & O'Mara 1991; Barklem & O'Mara 1998) when available. In the abundance analysis, we also include molecular line lists of CN (Jørgensen & Larsson 1990) and CO (Goorvitch 1994).

The line list is tested by determining abundances from high-quality spectra of α Boo (Hinkle et al. 1995) and five thick-disk stars. The thick-disk giants were observed with NIRSPEC in the same manner as for GC10812. The parameters and abundances of α Boo are from Ramírez & Allende Prieto (2011), and those of the thick-disk stars are from the APOGEE pipeline (Ahn et al. 2014). The parameter ranges of these test stars are $4150 < T_{eff}/K < 4750$, $1.5 < \log g < 2.5$, and $-0.5 < [Fe/H] < -0.1$. We find an excellent agreement, to within 0.05 dex, between the abundances we determined from the K band and these reference values. The line list has not yet been tested against supersolar-metalicity stars. Thus, the line list can with confidence be used for metal-poor to solar-metallicity cool stars.

4.3. Spectral Synthesis

We derive our target star's abundances by comparing the observed spectrum with synthesized spectra using the software *Spectroscopy Made Easy, SME* (Valenti &

Table 3
Line List

Element	Wavelength in Air (Å)	Exc. Pot. eV	log(gf) (cgs)
Mg I	21208.106	6.73	−0.821
Si I	21195.298	7.29	−0.425
Si I	21779.720	6.72	0.418
Si I	21819.711	6.72	0.087
Si I	21874.199	6.72	−0.731
Si I	21879.345	6.72	0.384
Si I	22537.593	6.62	−0.216
Ca I	22626.786	4.68	−0.281
Sc I	21730.452	1.44	−1.880
Sc I	21812.174	1.43	−1.490
Sc I	21842.781	1.43	−1.760
Sc I	22394.695	1.43	−1.180
Ti I	22632.743	1.88	−2.760
Fe I	21124.505	5.33	−1.647
Fe I	21238.509	4.96	−1.281
Fe I	21779.651	3.64	−4.298
Fe I	21894.983	6.13	−0.135
Fe I	22380.835	5.03	−0.409
Fe I	22392.915	5.10	−1.207
Fe I	22473.263	6.12	0.483
Fe I	22619.873	4.99	−0.362

Piskunov 1996, 2012; Piskunov & Valenti 2016). This program uses a grid of model atmospheres (MARCS spherical-symmetric, LTE model atmospheres; Gustafsson et al. 2008) in which it interpolates for a given set of fundamental parameters of the analyzed star. The spectral lines, which are used for the abundance analysis, are marked with masks in the pre-normalized observed spectra. SME then iteratively synthesizes spectra for the searched abundances, under a scheme to minimize the χ^2 when comparing with the observed spectra. In order to match our synthetic spectra with the observed ones, we also convolve the synthetic spectra with a Gaussian function of FWHM of 20 ± 0.5 km s^{-1}. This broadening accounts for the instrumental spectral resolution and the macroturbulence of the stellar atmosphere.

The abundances of the elements Fe, Mg, Si, Ca, Ti, and Sc are determined from carefully chosen lines. We have restricted our analysis to lines that are on the weak part of the curve of growth, i.e., with equivalent widths of $W < 250$ Å or $\log W/\lambda < -4.9$. This means that at our resolution of $R = 24{,}000$, there is an upper limit to the line depth of approximately 0.75 of the continuum. Lines deeper than this will certainly be saturated and will be not as sensitive to the abundance but at the same time more sensitive to the uncertain microturbulence parameters, ξ_{mic}. Our restriction of the analysis to weak lines will ensure a good measurement of the abundances. We also require that the spectral recording around the lines and the form of the continuum is of such high quality that the continuum is traceable.

---

[9] ABO stands for Anstee, Barklem, and O'Mara, authors of the papers describing the theory in Anstee & O'Mara (1991) and Barklem & O'Mara (1998).

Table 4
Uncertainties due to Uncertainties in the Stellar Parameters

Parameter	[Fe/H]	[Mg/Fe]	[Si/Fe]	[Ca/Fe]	[Ti/Fe]	[Sc/Fe]
$\Delta T_{\rm eff} = \pm 150$ K	<0.02	$+0.07$ -0.02	-0.04 $+0.10$	$+0.16$ -0.13	$+0.28$ -0.22	$+0.27$ -0.24
$\Delta \log g = \pm 0.3$ dex	<0.02	<0.02	$+0.07$ -0.03	-0.05 $+0.17$	-0.03 $+0.05$	-0.03 $+0.05$
$\Delta \xi_{\rm mic} = \pm 0.5$ km s^{-1}	-0.12 $+0.10$	$+0.02$ $+0.06$	-0.01 $+0.05$	-0.08 $+0.13$	-0.02 $+0.06$	-0.06 $+0.08$

The final line list is given in Table 3. In the table the wavelengths, excitation potential, and line strengths of the lines used for the abundance determination are given. The entire line list including all lines will be published elsewhere (B. Thorsbro et al. 2017, in preparation).

Examples of synthetic spectra are shown in Figure 4, and the derived abundances are given in Table 2. The Fe, Si, and Sc abundances are determined from eight, six, and four lines, respectively, whereas the Mg, Ca, and Ti abundances are determined from only one carefully chosen line each. This means that the former abundances are observationally better determined.

The uncertainties in the determination of the abundance ratios, for typical uncertainties in the stellar parameters, are ± 0.1 for [Fe/H], [Mg/Fe], and [Si/Fe], whereas it is ± 0.2 dex for [Ca/Fe] and ± 0.3 dex for [Ti/Fe] and [Sc/Fe]; see Table 4. In addition, we estimate random uncertainties of less than 0.05 dex due to the continuum placement. In Figure 4 we show the observed and our best-fit spectra, as well as synthetic spectra with ± 0.2 dex abundance variations with respect to the best-fit solution. The figure clearly shows that we can derive abundances with overall uncertainties smaller than 0.2 dex.

5. RESULTS

Our derived stellar parameters and their uncertainties for GC10812 are given in Table 2. We find that these parameters place the star in the appropriate location on the Hertzsprung–Russel diagram, as seen in Figure 5. It lies on the red giant branch appropriate for its metallicity, as demonstrated by plotting an old population with the 10 Gyr isochrones of Bressan et al. (2012).

Our derived abundances of Fe, Mg, Si, Ca, Ti, and Sc are given in Table 2. We have normalized our derived abundances to the solar abundances of Grevesse et al. (2007): $\log \varepsilon ({\rm Mg}) = 7.53$, $\log \varepsilon ({\rm Si}) = 7.51$, $\log \varepsilon ({\rm Ca}) = 6.31$, $\log \varepsilon ({\rm Sc}) = 3.17$, $\log \varepsilon ({\rm Ti}) = 5.02$, and $\log \varepsilon ({\rm Fe}) = 7.45$.

Typical internal errors in the derived stellar abundances are a few hundredths of dex, while the systematic uncertainties due to different assumptions for the stellar parameters are detailed in Table 4 and, on average, amount to 0.1–0.2 dex, often dominated by one of the uncertainties in the stellar parameters.

The derived [α/Fe] abundance ratios are plotted in Figure 6, together with the corresponding measurements of different samples of giants in the bulge from Gonzalez et al. (2011) and Johnson et al. (2014) by means of optical spectroscopy, as well as measurements in low-latitude (innermost 2°) fields from Rich et al. (2007, 2012) and Ryde et al. (2016) by using H- and K-band IR spectroscopy. In Figure 6 we also reported the measurements of some low-mass giants in the Galactic center region from Ryde & Schultheis (2015) and the average abundance ratios of the three stellar populations of Terzan 5 at $(l, b) = (3°.8, +1°.7)$ from Origlia et al. (2011, 2013).

We find that the [α/Fe] abundance ratios of GC10812 are consistent with an enhancement between a factor of two and three with respect to the solar values and fully consistent with the values measured in bulge and Galactic center giants with subsolar metallicities.

6. DISCUSSION

The best constraint of the 3D location of GC10812 is at 1.5 pc distance from the Sgr A* in projected distance on the sky and 26^{+54}_{-16} pc distance in the line of sight in front of the Galactic center. The nuclear cluster has a half-light radius of $178'' \pm 51'' \sim 7 \pm 2$ pc (Fritz et al. 2016), but the nuclear disk extends to about 230 pc (Launhardt et al. 2002). The dynamics of the star is typical for a Galactic center star, and our orbit calculations show that the star's orbit is constrained within the nuclear disk.

The kinematics strongly favor a Galactic center origin, and it is thus rather certain that the star belongs to a nuclear component. The probability of the star being a stray bulge giant is low since most bulge giants are more metal-rich and [Fe/H] ~ -1 stars are rare in the bulge (Ness & Freeman 2016). Based on the kinematics and metallicity, the probability of the star being a halo giant is also low since at least in the solar vicinity the halo metallicity in the mean is typically [Fe/H] ~ -1.6, not -1 (Ryan & Norris 1991). The relative number density of halo stars in the Galactic center is difficult to estimate, since there are no measurements of the halo quantitatively even within 8 kpc. Extrapolation can obtain a relevant mass in the center when a broken power law like, for example, that in Bland-Hawthorn & Gerhard (2016) is used. However, when other parameterizations are used, like an Einasto profile (Sesar et al. 2013; Xue et al. 2015), the obtained mass is much smaller and irrelevant. Also, from a theoretical standpoint a flatter profile is expected, since it is difficult for dwarf galaxies, which probably form the main contributor to the halo, to reach the center of the Milky Way. For example, Bullock & Johnston (2005) measure, in their model, a slope of -1 between 3 and 10 kpc, flatter than farther out. In summary, we conclude that the probability of GC10812 being a halo star is low.

The metallicity of GC10812 is lower than that of most stars in the inner bulge. Rich et al. (2007, 2012) find, for example, a dispersion of approximately 0.1 dex around [Fe/H] $= -0.05$ to -0.15. The more recent works of Schultheis et al. (2015) and Ryde et al. (2016) found, in addition, also some metal-poor stars with [Fe/H] ≈ -1. They are, with $|b| > 0.4°$, all located outside the nuclear disk. Within the nuclear components (disk and cluster) Cunha et al. (2007) find a total spread of 0.16 dex around [Fe/H] $= +0.14$ for the luminous giants and super-giants located within 2.2 pc of the Galactic center. Further, Carr et al. (2000), Ramírez et al. (2000b), and Davies et al. (2009) analyzed high-resolution spectra of supergiant stars in the
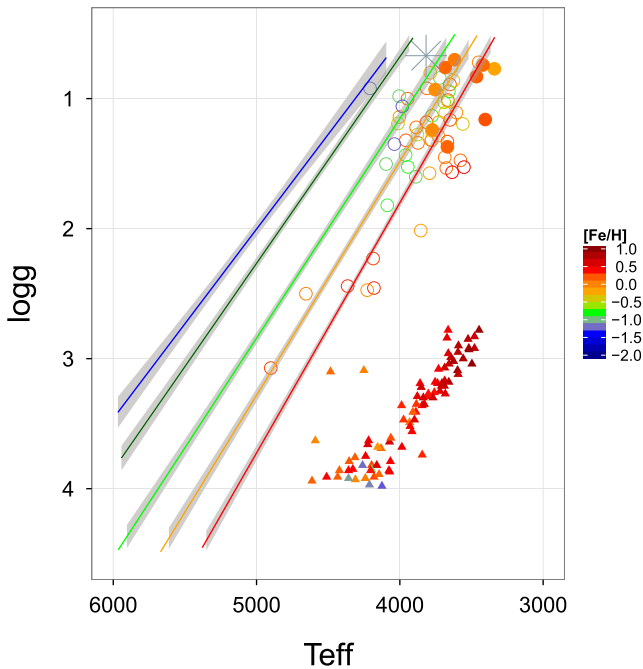
Figure 5. Logarithm of the surface gravities of inner bulge stars plotted vs. their effective temperatures and color-coded by their metallicities. The big star is the metal-poor star GC10812 discussed in this paper. The selection of stars in the inner 3° of the bulge from the literature are marked by open circles for the stars from Ryde et al. (2016) and Schultheis et al. (2015), by filled circles for the stars within 10 pc projected galactocentric distance from Ryde & Schultheis (2015), and by triangles for the stars discussed in Do et al. (2015). Superimposed are also the 10 Gyr PARSEC isochrones (Bressan et al. 2012) with the corresponding color of the metallicity.

Galactic center, finding near-solar metallicity. Similarly, Ryde & Schultheis (2015) at about 4′ distance from Sgr A* also only detect a metal-rich component with a total spread of 0.15 dex around [Fe/H] = +0.11.

The location of the [α/Fe] abundance ratios versus metallicity for the giant GC10812 is that expected for the metal-poor population in the outer bulge. The [Mg/Fe] and [Si/Fe] trends of the inner bulge are tight and are indistinguishable from the outer bulge trend, within uncertainties. Although with a larger scatter, this is also true for the [Ca/Fe] abundances for giants in the central regions (Cunha et al. 2007; Origlia et al. 2011; Johnson et al. 2014; Ryde et al. 2016). It can, however, be noted that they all follow a higher trend than that determined by Bensby et al. (2013). This might (but not necessarily) arise from greater errors ultimately attributable to the higher uncertainties based on the Ca determination based on the giant star spectra as compared with those based on dwarf spectra (see also the discussion in Gonzalez et al. 2011). Scrutinizing the Ca line used, using more Ca lines, comparing with detailed galactic chemical evolution models, and observing more stars will be needed to investigate and understand the true nature of the [Ca/Fe] trend. Our [Ti/Fe] determination also has a high uncertainty, mainly arising from the uncertainty in the effective temperature. The value is, however, consistent within errors with the other bulge stars too. Thus, within the uncertainties, the [α/Fe] we measure for GC10812 cannot be claimed to be different from the rest of the bulge.

The log g versus $T_{\rm eff}$ location of GC10812 is indicated in Figure 5 with a large asterisk. Superimposed are isochrones color-coded for different metallicities (Bressan et al. 2012). We

assume here an age of 10 Gyr. The red line shows the most metal-rich isochrone (+0.7 dex). Based on its apparent luminosity, its kinematic membership to one of the nulcear components, its low metallicity, our independent determination of its effective temperature and surface gravity, and its high α abundance, we are confident that GC10812 is consistent with being a low-mass, old red giant star in the vicinity of the nuclear cluster.

In the figure we also plot the locations for a sample of stars in the inner 3° from the Galactic center from Ryde & Schultheis (2015), Ryde et al. (2016), Schultheis et al. (2015), and Do et al. (2015). The typical uncertainties of temperatures are about ±150 K, while the errors in log g can be on the order of 0.3–0.5 dex as those were determined photometrically. We note that the isochrones predict too high temperatures, for a given surface gravity, for the most metal-rich stars (>0.5 dex). One should, however, be aware of the fact that everything at metallicity >+0.5 dex needs still to be understood: the metallicities themselves, model atmospheres, and isochrones are all very uncertain and mostly calibrated by extrapolation. Thus, it could be possible that the log g determination of the most metal-rich stars is ∼0.3–0.5 dex too high.

Whereas the M giants from Ryde & Schultheis (2015), Ryde et al. (2016), and Schultheis et al. (2015) are situated along the isochrone sequence in Figure 5, the location of the Do et al. (2015) stars is not compatible with the indicated location of the RGB branch from the PARSEC isochrones. These stars are plotted as triangles. As their extinction is typically that of stars in the Galactic center, we believe that their surface gravities are about two to three order of magnitudes too high. Also, the metal-poor stars discussed in Do et al. (2015) are orders of magnitude away from the expected isochrones.

The work of Do et al. (2015) obtained integral-field, moderate-resolution spectroscopy for scores of stars in the central cluster behind adaptive optics (AO). They did not claim to undertake a full high-resolution abundance analysis and were aware of potentially significant uncertainties in their methods. Their stated uncertainty in log g is 0.91 dex. The main effect of decreasing the surface gravity in a synthetic spectrum calculation is the decreased continuous opacity, which generally increases the line strengths. In the simultaneous fit of the stellar parameters by Do et al. (2015), the temperature and metallicity determinations might therefore also be affected by this large uncertainty. We agree with the assessment of Do et al. (2015) that additional observations at high spectral resolution would be required to confirm the low metallicities ([Fe/H] ∼ −1) claimed for the five stars in the nuclear cluster. Likewise, the high-metallicity stars found by Do et al. (2015), which have nominal metallicities up to [Fe/H] = +1.0 dex, need to be confirmed.

The similarity between GC10812 and the rest of the inner bulge would suggest a homogeneous star formation history in the entire bulge. There is a clear connection with the bulge and the Galactic center. Thus, our results argue for the Galactic center being in the context of the bulge over most of its history rather than very distinct.

7. CONCLUSIONS

In targeting the Milky Way nuclear star cluster we have observed the most metal-poor giant (GC10812) yet in the vicinity of the Galactic center. A careful analysis of its three-
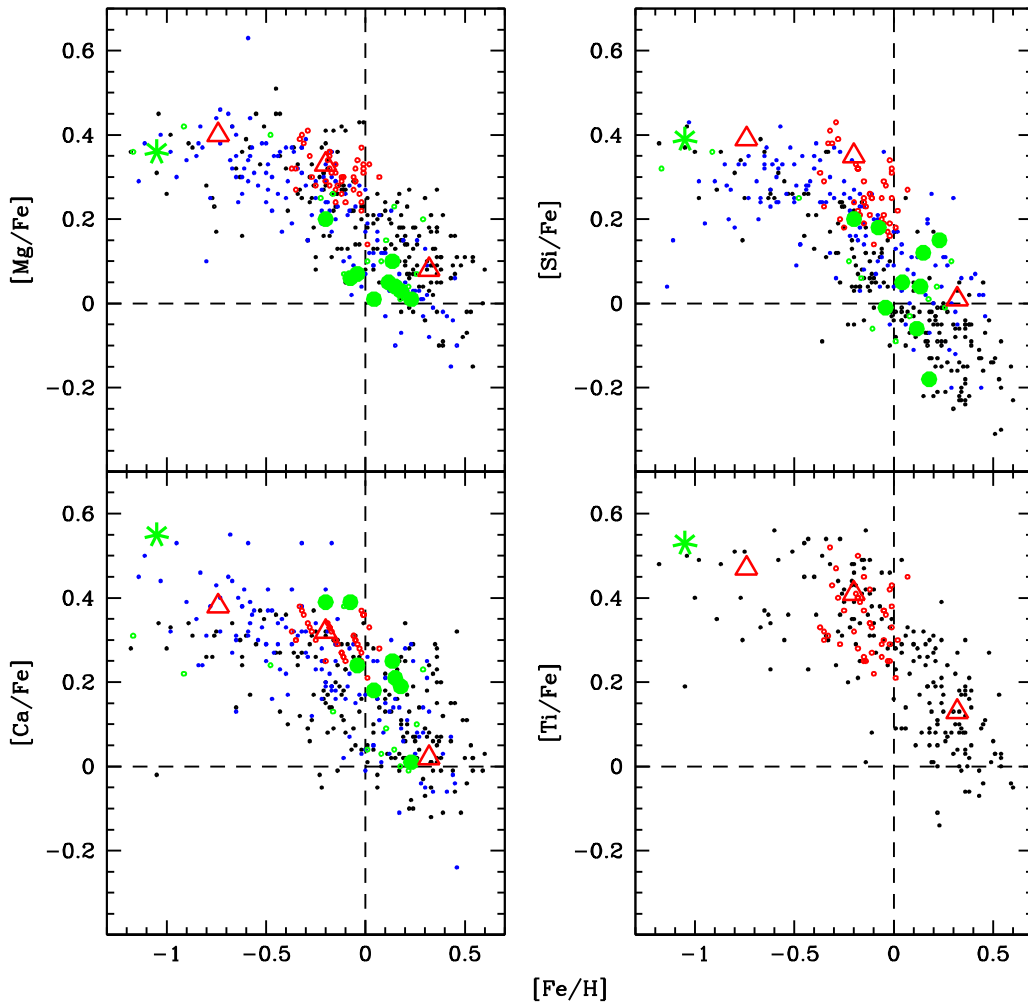
Figure 6. Abundance ratios of [Mg/Fe], [Si/Fe], [Ca/Fe], and [Ti/Fe] vs. [Fe/H] for GC10812 (big green star) and different samples of bulge and Galactic center giants: Gonzalez et al. (2011) (black dots), Johnson et al. (2014) (blue dots) in the outer bulge from optical spectroscopy, Rich et al. (2007, 2012) (red circles) and Ryde et al. (2016) (green circles) in low-latitude bulge fields, and Ryde & Schultheis (2015) (big green dots) in the Galactic center region from IR spectroscopy. The average abundance ratios of the three stellar populations of Terzan 5 from Origlia et al. (2011, 2013) (big red triangles) are also plotted for comparison. We have rescaled all the abundances to the same solar reference of Grevesse et al. (2007).

dimensional location locates it at 26^{+54}_{-16} pc in front of the Galactic center and at a projected distance of 1.5 pc to the northwest. This line-of-sight position and orbit integration make it unlikely that the star belongs in the most central component, the nuclear cluster. However, the orbit integration also shows that the star very likely does not leave the nuclear disk. Thus, the star very likely belongs to a nuclear component.

The metallicity and abundances are determined from a detailed abundance analysis based on $R = 24,000$ Keck/NIRSPEC spectra. The [Fe/H] $= -1.05 \pm 0.10$ is the lowest measured and confirmed metallcitiy of a star from the nuclear components. It is unexpected and differs from earlier measurements. We can, however, still conclude that there is no evidence hitherto that there are metal-poor stars (e.g., originating in globular clusters inspiraling to the Galactic center; Tremaine et al. 1975; Capuzzo-Dolcetta & Miocchi 2008) in the nuclear star cluster. The [α/Fe]-element enhancement of $\sim +0.4$ follows the trend of the outer bulge.

GC10812 is by virtue of its 3D kinematics a likely member of the central disk/cluster system. It also exhibits the metal-poor, alpha-enhanced hallmarks of an old, metal-poor giant. The existence of an old population in the Galactic center has

been well established from the robust presence of a red clump population (Figer et al. 2004), as well as the analysis of star formation history by Pfuhl et al. (2011). It will be important going forward to explore the full abundance distribution of this old population, as well as that of the $\sim 10^8$ yr population responsible for the supergiants. Such studies will lay the foundation for applying models of chemical evolution to this very interesting region of the Milky Way.

We have demonstrated that K-band spectroscopy of individual giants at high spectral resolution offers a path forward enabling exploration of the chemistry of the central cluster. This has the potential to elucidate the system's star formation and enrichment history, as well as its relationship with the central 100 pc of the bulge/bar system.

REFERENCES

Ahn, C. P., Alexandroff, R., Allende Prieto, C., et al. 2014, ApJS, 211, 17
Anstee, S. D., & O'Mara, B. J. 1991, MNRAS, 253, 549
Baade, W. 1951, POMic, 10, 7
Barklem, P. S., & O'Mara, B. J. 1998, MNRAS, 300, 863
Bensby, T., Yee, J. C., Feltzing, S., et al. 2013, A&A, 549, A147
Bland-Hawthorn, J., & Gerhard, O. 2016, ARA&A, 54, 529
Blum, R. D., Ramírez, S. V., Sellgren, K., & Olsen, K. 2003, ApJ, 597, 323
Bonnet, H., Ströbele, S., Biancat-Marchet, F., et al. 2003, Proc. SPIE, 4839, 329
Bressan, A., Marigo, P., Girardi, L., et al. 2012, MNRAS, 427, 127
Bullock, J. S., & Johnston, K. V. 2005, ApJ, 635, 931
Capuzzo-Dolcetta, R., & Miocchi, P. 2008, ApJ, 681, 1136
Cardelli, J. A., Clayton, G. C., & Mathis, J. S. 1989, ApJ, 345, 245
Carr, J. S., Sellgren, K., & Balachandran, S. C. 2000, ApJ, 530, 307
Chatzopoulos, S., Fritz, T. K., Gerhard, O., et al. 2015a, MNRAS, 447, 948
Chatzopoulos, S., Gerhard, O., Fritz, T. K., et al. 2015b, MNRAS, 453, 939
Cunha, K., Sellgren, K., Smith, V. V., et al. 2007, ApJ, 669, 1011
Davies, B., Origlia, L., Kudritzki, R.-P., et al. 2009, ApJ, 694, 46
Do, T., Kerzendorf, W., Winsor, N., et al. 2015, arXiv:1506.07891
Eisenhauer, F., Abuter, R., Bickert, K., et al. 2003, Proc. SPIE, 4841, 1548
Figer, D. F., Rich, R. M., Kim, S. S., Morris, M., & Serabyn, E. 2004, ApJ, 601, 319
Fritz, T. K., Chatzopoulos, S., Gerhard, O., et al. 2016, ApJ, 821, 44
Fritz, T. K., Gillessen, S., Dodds-Eden, K., et al. 2011, ApJ, 737, 73
Fulbright, J. P., McWilliam, A., & Rich, R. M. 2006, ApJ, 636, 821
Gonzalez, O. A., Rejkuba, M., Zoccali, M., et al. 2011, A&A, 530, A54
Gonzalez, O. A., Zoccali, M., Vasquez, S., et al. 2015, A&A, 584, A46
Goorvitch, D. 1994, ApJS, 95, 535
Grevesse, N., Asplund, M., & Sauval, A. J. 2007, SSRv, 130, 105
Gustafsson, B., Edvardsson, B., Eriksson, K., et al. 2008, A&A, 486, 951
Hinkle, K., Wallace, L., & Livingston, W. C. 1995, Infrared Atlas of the Arcturus Spectrum, 0.9–5.3 microns (San Francisco, CA: ASP) (http://adsabs.harvard.edu/abs/1995iaas.book.....H)
Houdashelt, M. L., Bell, R. A., & Sweigart, A. V. 2000, AJ, 119, 1448
Howes, L. M., Casey, A. R., Asplund, M., et al. 2015, Natur, 527, 484
Johnson, C. I., Rich, R. M., Fulbright, J. P., Valenti, E., & McWilliam, A. 2011, ApJ, 732, 108
Johnson, C. I., Rich, R. M., Kobayashi, C., et al. 2013, ApJ, 765, 157
Johnson, C. I., Rich, R. M., Kobayashi, C., Kunder, A., & Koch, A. 2014, AJ, 148, 67
Jørgensen, U. G., & Larsson, M. 1990, A&A, 238, 424

Kim, S., Prato, L., & McLean, I. 2015, REDSPEC: NIRSPEC Data Reduction, Astrophysics Source Code Library, ascl:1507.017
Koch, A., McWilliam, A., Preston, G. W., & Thompson, I. B. 2016, A&A, 587, A124
Kupka, F., Piskunov, N., Ryabchikova, T. A., Stempels, H. C., & Weiss, W. W. 1999, A&AS, 138, 119
Kupka, F. G., Ryabchikova, T. A., Piskunov, N. E., Stempels, H. C., & Weiss, W. W. 2000, BaltA, 9, 590
Launhardt, R., Zylka, R., & Mezger, P. G. 2002, A&A, 384, 112
Lawrence, A., Warren, S. J., Almaini, O., et al. 2013, yCat, 2319, 0
Livingston, W., & Wallace, L. 1991, An Atlas of the Solar Spectrum in the Infrared from 1850 to 9000 cm^{-1} (1.1 to 5.4 micrometer), NSO Tech. Rep. (Tucson, AZ: National Solar Observatory, National Optical Astronomy Observatory) (http://adsabs.harvard.edu/abs/1991aass.book.....L)
Matsunaga, N., Kawadu, T., Nishiyama, S., et al. 2009, MNRAS, 399, 1709
McLean, I. S. 2005, in High Resolution Infrared Spectroscopy in Astronomy, ed. H. U. Käufl, R. Siebenmorgen, & A. F. M. Moorwood (Berlin: Springer), 25
Nassau, J. J., & Blanco, V. M. 1958, ApJ, 128, 46
Ness, M., & Freeman, K. 2016, PASA, 33, e022
Ness, M., Freeman, K., Athanassoula, E., et al. 2013, MNRAS, 430, 836
Nishiyama, S., Tamura, M., Hatano, H., et al. 2009, ApJ, 696, 1407
Omont, A., Ganesh, S., Alard, C., et al. 1999, A&A, 348, 755
Origlia, L., Massari, D., Rich, R. M., et al. 2013, ApJL, 779, L5
Origlia, L., Rich, R. M., Ferraro, F. R., et al. 2011, ApJL, 726, L20
Pehlivan, A., Nilsson, H., & Hartman, H. 2015, A&A, 582, A98
Pfuhl, O., Fritz, T. K., Zilka, M., et al. 2011, ApJ, 741, 108
Piskunov, N., & Valenti, J. A. 2016, arXiv:1606.06073
Piskunov, N. E., Kupka, F., Ryabchikova, T. A., Weiss, W. W., & Jeffery, C. S. 1995, A&AS, 112, 525
Ramírez, I., & Allende Prieto, C. 2011, ApJ, 743, 135
Ramirez, S. V., Depoy, D. L., Frogel, J. A., Sellgren, K., & Blum, R. D. 1997, AJ, 113, 1411
Ramírez, S. V., Sellgren, K., Carr, J. S., et al. 2000a, ApJ, 537, 205
Ramírez, S. V., Stephens, A. W., Frogel, J. A., & DePoy, D. L. 2000b, AJ, 120, 833
Rich, R. M. 1988, AJ, 95, 828
Rich, R. M., Origlia, L., & Valenti, E. 2007, ApJL, 665, L119
Rich, R. M., Origlia, L., & Valenti, E. 2012, ApJ, 746, 59
Ryabchikova, T., Piskunov, N., Kurucz, R. L., et al. 2015, PhyS, 90, 054005
Ryabchikova, T. A., Piskunov, N. E., Kupka, F., & Weiss, W. W. 1997, BaltA, 6, 244
Ryan, S. G., & Norris, J. E. 1991, AJ, 101, 1865
Ryde, N., & Schultheis, M. 2015, A&A, 573, A14
Ryde, N., Schultheis, M., Grieco, V., et al. 2016, AJ, 151, 1
Schödel, R., Feldmeier, A., Kunneriath, D., et al. 2014, A&A, 566, A47
Schödel, R., Najarro, F., Muzic, K., & Eckart, A. 2010, A&A, 511, A18
Schultheis, M., Chen, B. Q., Jiang, B. W., et al. 2014, A&A, 566, A120
Schultheis, M., Cunha, K., Zasowski, G., et al. 2015, A&A, 584, A45
Schultheis, M., Ryde, N., & Nandakumar, G. 2016, A&A, 590, 13
Sesar, B., Ivezić, Ž., Stuart, J. S., et al. 2013, AJ, 146, 21
Tiede, G. P., Frogel, J. A., & Terndrup, D. M. 1995, AJ, 110, 2788
Tody, D. 1993, in ASP Conf. Ser. 52: Astronomical Data Analysis Software and Systems II, ed. R. J. Hanisch, R. J. V. Brissenden, & J. Barnes (San Francisco, CA: ASP), 173
Tremaine, S. D., Ostriker, J. P., & Spitzer, L., Jr. 1975, ApJ, 196, 407
Tsuji, T. 2008, A&A, 489, 1271
Valenti, J. A., & Piskunov, N. 1996, A&AS, 118, 595
Valenti, J. A., & Piskunov, N. 2012, SME: Spectroscopy Made Easy, Astrophysics Source Code Library, ascl:1202.013
Xue, X.-X., Rix, H.-W., Ma, Z., et al. 2015, ApJ, 809, 144
Zoccali, M., Hill, V., Lecureur, A., et al. 2008, A&A, 486, 177